Applied Physics Letters ARTICLE pubs.aip.org/aip/apl

Molecular engineering of PEDOT:PSS for enhancing open-circuit voltage in organic/silicon heterojunction solar cells

Cite as: Appl. Phys. Lett. **127**, 261601 (2025); doi: 10.1063/5.0306461
Submitted: 10 October 2025 · Accepted: 11 December 2025 ·
Published Online: 30 December 2025

Leiming Yu, Rui Yang, Xiangdong Duan, Zhuo Wu, Suicai Zhang,[a] Xiaohui Song, Yurong Jiang, and Congxin Xia[a]

AFFILIATIONS

School of Physics, Henan Key Laboratory of Advanced Semiconductor & Functional Device Integration, Henan Normal University, Xinxiang 453007, China

[a]Authors to whom correspondence should be addressed: zhangsuicai@htu.edu.cn and xiacongxin@htu.edu.cn

ABSTRACT

Poly(3,4-ethylenedioxythiophene):poly(styrenesulfonate) (PEDOT:PSS)/silicon (Si) heterojunction solar cells (HSCs) have garnered extensive interest owing to their potential for high efficiency and low cost. However, their performance is constrained by a limited open-circuit voltage (V_{OC}). In this manuscript, PEDOT:PSS films endowed with both high conductance and high work function via an alcohol-doping-based molecular engineering strategy were applied to induce strong inversion layers on the n-Si surface and generate large built-in voltage in HSCs. This molecular engineering strategy enables precise modulation of PEDOT:PSS molecular building blocks, achieving a work function tuning range from 4.81 to 4.93 eV while retaining high conductivity exceeding 650 S/cm. A photovoltaic device with alcohol-doped PEDOT:PSS delivers a large V_{OC} of 0.66 V without additional modifications and a power conversion efficiency of 12.80%. This study on the molecular engineering of PEDOT:PSS establishes an effective and simplified pathway for fabricating PEDOT:PSS/Si HSCs with high V_{OC}.

Among various organic materials, the conjugated polymer poly(3,4-ethylenedioxythiophene):poly(styrene sulfonate) (PEDOT:PSS) has become a highly competitive candidate and is widely used in silicon/organic heterojunction solar cells, owing to its high conductivity, excellent transparency, promising antireflection properties, commercial availability, and ease of processability.[1–10] The PEDOT:PSS/Si heterojunction, formed by combining PEDOT:PSS with crystalline silicon and designed to replace the traditional homogeneous buried junction in solar cells, can be constructed without high-temperature doping diffusion processing.[11,12] Additionally, PEDOT:PSS/n-Si HSCs based on this heterojunction are usually fabricated through a full-solution approach in the atmosphere, without using an a-Si:H passivation layer (dependent on vacuum technologies such as plasma-enhanced chemical vapor deposition), thus exhibiting a remarkable low-cost advantage.[13,14] Owing to its simple fabrication process and the excellent optoelectronic properties of silicon, the PEDOT:PSS/Si HSCs has become a promising competitor among emerging photovoltaic technologies.[2] Currently, the power conversion efficiencies (PCEs) of PEDOT:PSS/n-Si HSCs have undergone significant improvement and exceeded 18%.[15,16] However, although many silicon surface passivation technologies, back-surface field formation methods, and conformal contact strategies have been used to improve open-circuit voltage (V_{OC}) of these solar cells, the V_{OC} is still below 630 mV under most conditions, which still lags far behind theoretical simulations and crystalline Si solar cells.[17–20] Therefore, how to achieve a high V_{OC} without increasing the complexity of the preparation process is still an obstacle that needs to be conquered.[21–23]

The V_{OC} is fundamentally determined by PEDOT:PSS/n-Si heterojunction quality. The heterojunction quality relies on both the PEDOT:PSS layer itself and its interface with Si.[4,8,22–24] Achieving a higher V_{OC} hinges on optimizing the work function of PEDOT:PSS to maximize the band bending at the silicon interface while maintaining high electrical conductivity for effective charge carrier transport.[25,26] Conventional methods to increase the work function include surface transfer doping and classical doping.[10,27] Among these, surface transfer doping involves coating PEDOT:PSS film with high work function materials. However, the scarcity of suitable materials and the complexity of the fabrication process (such as vacuum evaporation) limit its further development.[28,29] On the contrary, classical doping is realized by doping additives (such as CuPc, Nafion, MoO_3, and V_2O_5) into the PEDOT:PSS precursor solution.[11,21,28,30,31] Nevertheless, this approach

suffers from low doping efficiency, and high-concentration doping will significantly degrade the optoelectronic properties of the PEDOT:PSS.[32] So far, it is the key issue to find a facile, precise, and effective strategy to adjust the work function without a complex process or damage to the photoelectric properties of the PEDOT:PSS film.

In this paper, we present a straightforward yet effective molecular engineering method that utilizes alcohols with varying reducibility to modify PEDOT:PSS, thereby enhancing the film's conductivity and fine-tuning its work function. As a result, the work function of PEDOT:PSS can be engineered to span from 4.81 to 4.93 eV, while sustaining conductivity above 650 S/cm. PEDOT:PSS/Si photovoltaic device characterization reveals that the elevated work function of PG-modified PEDOT:PSS films induces a robust inversion layer on the Si surface, thereby significantly enhancing the built-in potential and reducing interface recombination. Through the optimization of the PEDOT:PSS/Si heterojunction interface, a record-high V_{OC} of 0.66 V was ultimately achieved.

Figure 1(a) presents the structure of the PEDOT:PSS molecule, which is composed of PEDOT and PSS linked together by electrostatic interaction. In the PEDOT molecule, the proportion of three functional groups—benzene (B) structure and quinoid (Q_1 and Q_2)—determines its conductivity.[33] Figure 1(b) shows the molecular structures of alcohols with different reducibility [propylene glycol (PG), ethylene glycol (EG), and D-sorbitol (D-S)], which are used to regulate the molecular structure of PEDOT:PSS.[34] Figure 1(c) presents schematic diagrams illustrating the tendency of molecular structural transformation under the action of reducing alcohols. As shown in Fig. 1(c), low reducibility alcohols (LRA) preferentially facilitate the transformation of the benzene (B) structure in PEDOT to the Q_2 form, whereas high reducibility alcohols (HRA) direct this conversion toward the Q_1 state. The quinoid structure is widely recognized as the primary contributor to higher conductivity, and it tends to form linear or fibrillary-like morphologies within the film, and the coil-like benzene structure present in the film gives rise to low conductance.[13,35,36] In addition, modification with an alcohol of appropriate reducibility induces the dissociation of PEDOT:PSS and disrupts the original core–shell structure, promoting the formation of more extended PEDOT chains and establishing continuous conductive pathways, as shown in Fig. 1(c).[37–39]

Raman spectroscopy in the wavenumber range of 1340–1600 cm^{-1} was employed to characterize the influence of alcohols on the molecular structure of PEDOT:PSS.[40] As shown in Fig. 1(d), the pristine PEDOT:PSS exhibits three characteristic groups after peak deconvolution: (i) the peak at 1457 cm^{-1} is associated with the benzene conformation (B) with symmetric C_a=C_b (-O) stretching, (ii) the peak at approximately 1405 cm^{-1} is related to an asymmetric quinoid state (Q_1), and (iii) the 1435 cm^{-1} feature corresponds to the quinoid conformation (Q_2) with symmetric C_a-C_b (-O) stretching.[41–43] The electrical properties of PEDOT:PSS films are mainly determined by the proportions of the three components.[44] As shown in the deconvolution results of the Raman spectra [Figs. 1(d), 1(e), and S1], the relative proportions of the B, Q_1, and Q_2 structures undergo a significant change after alcohol modification. The components of the B structure gradually convert to the Q structures. The proportion of the benzene (B) structure in the PEDOT:PSS films with different alcohols modified does not change significantly, ranging from 3% to 5%, but the proportions of the two quinoid structures show distinct differences. The PG-modified film exhibits the highest Q_2 proportion (65%). Meanwhile, the content of the Q_1 shows a gradual increase with the enhanced reducibility of the alcohols used.

The composition of PEDOT:PSS was analyzed through XPS measurement, as shown in Figs. 1(f), 1(g), and S1. The S 2p core-level spectra exhibit two prominent contributions: one originating from PEDOT on the low binding energy (BE) side and the other deriving from PSS on the high BE side.[45,46] It can be seen that when normalization is performed according to the highest peak of PEDOT, the -S-/SO_3H ratio in the alcohol modified films are higher than that in the original film. This suggests a reduction in the PSS component after alcohol modification, which is attributed to its dissociation from PEDOT. The content of PSS components in different alcohol-modified films also varies. This is due to the different redox properties or hydrophilicity of the modified solvent, resulting in different degrees of dissociation of PEDOT:PSS.[37] These Raman and XPS experimental results confirm the hypothesis regarding molecular structural transformation presented in Fig. 1(c).

The surface morphology analysis was performed by scanning electron microscopy (SEM) and atomic force microscopy (AFM). Figure 2(a) shows an original PEDOT:PSS film, in which there is no rearrangement between PEDOT and PSS, and PEDOT:PSS aggregates in a granular structure. In contrast, the morphology of the alcohol-modified PEDOT:PSS films [Figs. 2(b)–2(d)] undergoes drastic changes, revealing a more obvious fibrous structure. The bright fibrous region is the highly conductive PEDOT, while the darker region is the insulating PSS. The results clearly show that alcohol modification leads to a change in the composition of PEDOT:PSS, from a curled shape rich in benzene structure to a fibrous shape rich in quinoid structure,[47] resulting in a slight increase in the root mean square (RMS) roughness of the modified film, as shown in the AFM image in Figs. 2(e)–2(h).

The electrical properties of alcohol-modified PEDOT:PSS films were characterized by van der Pauw–Hall measurements. Figure 3(a) presents the conductivity of PEDOT:PSS films as a function of the doping concentration of alcohols in the PEDOT:PSS precursor solution. The conductivity values of the PEDOT:PSS films increase significantly with the addition of low-concentration alcohols, uniformly reaching a plateau when the alcohol concentration exceeds 5 wt. %. PG, EG, and D-S modified PEDOT:PSS films all exhibit superior conductivity exceeding 650 S/cm. The corresponding carrier concentration and mobility are shown in Figs. 3(b) and 3(c). The D-S modified PEDOT:PSS films exhibit an ultra-high carrier concentration of 10^{21} cm^{-3}, while the PG-modified films demonstrate a high carrier mobility of 5.37 $cm^2V^{-1}s^{-1}$. We speculate that the discrepancy in these electrical properties is primarily attributed to variations in the internal structure of PEDOT:PSS molecules.

To fabricate unetched photovoltaic devices with high sunlight utilization efficiency, an optical model was constructed to simulate the reflection spectra of the solar cell devices. Figure 3(d) presents the optical constants of PEDOT:PSS films with different alcohols doped in the PEDOT:PSS precursor solution. Figure 3(e) shows a reflectance map of semi-finished devices as a function of PEDOT:PSS thickness and incident wavelength. As shown in Fig. 3(e), the reflectivity of the device varies approximately periodically with the thickness of the PEDOT:PSS film. This phenomenon arises from the interference between the reflected light at the PEDOT:PSS/air interface and that at the PEDOT:PSS/Si interface. It can be concluded that the semi-finished

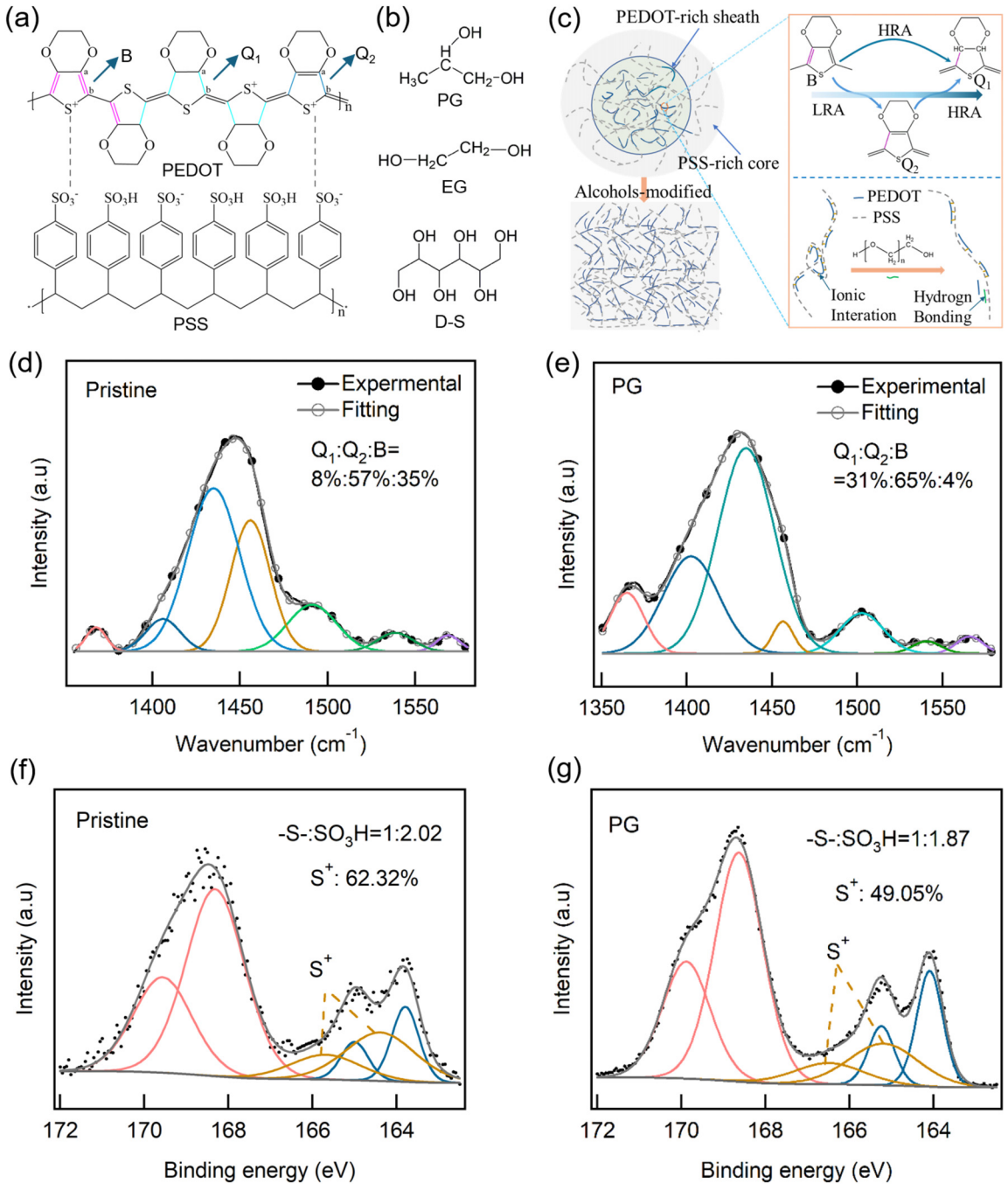

FIG. 1. (a) Schematic structure of PEDOT:PSS. (b) Chemical structures of the different alcohols. (c) Molecular structural schemes of the PEDOT chain (benzene, intermediate, and quinoid forms) illustrating their transformation tendency and the dissociation mechanism of PEDOT:PSS under the action of reducing alcohols. (d) and (e) Peak-fitting analysis of the Raman spectra and [(f) and (g)] XPS spectra of the S 2p core levels for the PEDOT:PSS films.

devices exhibiting the weakest reflectivity should feature a PEDOT:PSS film with a thickness of approximately 90 nm. Figure 3(f) presents the reflection spectra of PEDOT:PSS films modified with different alcohols, with a thickness of approximately 90 nm.

Based on the results of electrical and optical properties characterization, we fabricated PEDOT:PSS/Si HSCs using pristine and three alcohols-modified types of PEDOT:PSS films. Figure 4(a) shows the device configuration of PEDOT:PSS/Si HSCs, which is composed of

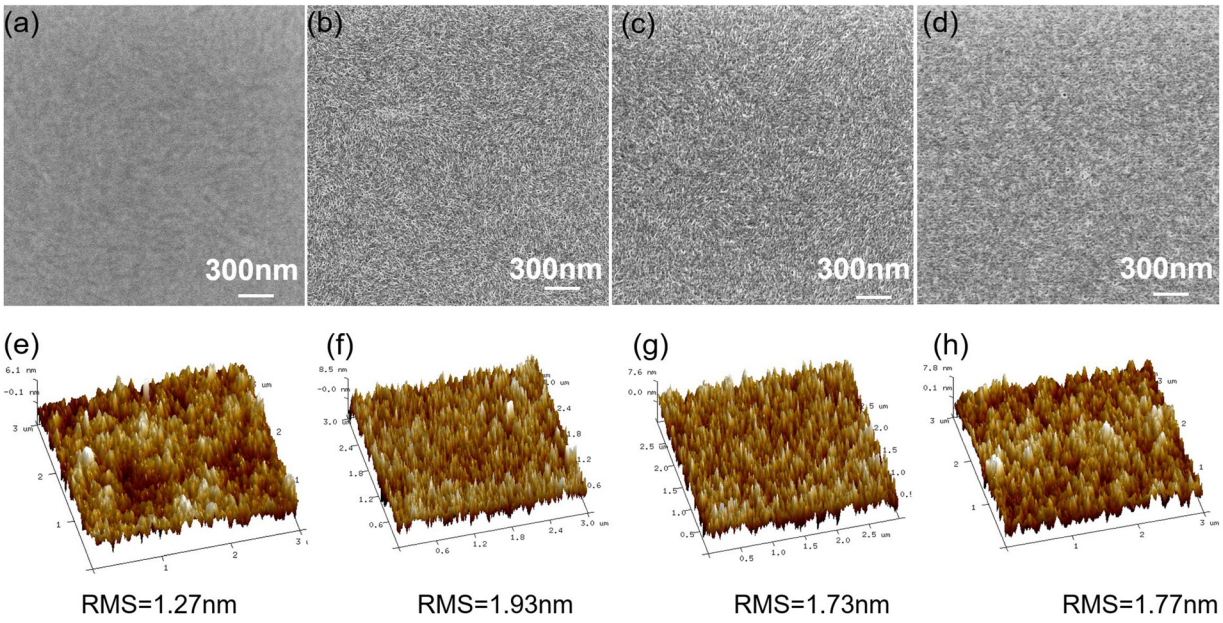

FIG. 2. SEM and AFM images of various PEDOT:PSS films on planar Si substrate: (a) and (e) pristine PEDOT:PSS film; (b) and (f) PEDOT:PSS film with EG doping; (c) and (g) PEDOT:PSS film with PG doping; and (d) and (h) PEDOT:PSS film with D-S doping.

an Ag-grid (200 nm), a PEDOT:PSS film (∼90 nm), an n-type Si wafer (300 μm, 0.05–0.1 Ω·cm), Phenyl-C61-butyric acid methyl ester (PCBM, ∼30 nm), and Al electrode (100 nm). Figure 4(b) shows the J–V characteristic curves of PEDOT:PSS/n-Si HSCs under AM1.5G simulated solar light. For all four types of solar cells, the devices with PG-modified PEDOT:PSS exhibit the best performance, with a PCE of 12.80% and a V_{OC} of up to 0.66 V (detailed photovoltaic parameters are presented in Table S2). Figure 4(c) presents the dark current density of the corresponding devices. Devices fabricated with PG-modified PEDOT:PSS films exhibit the lowest dark current,

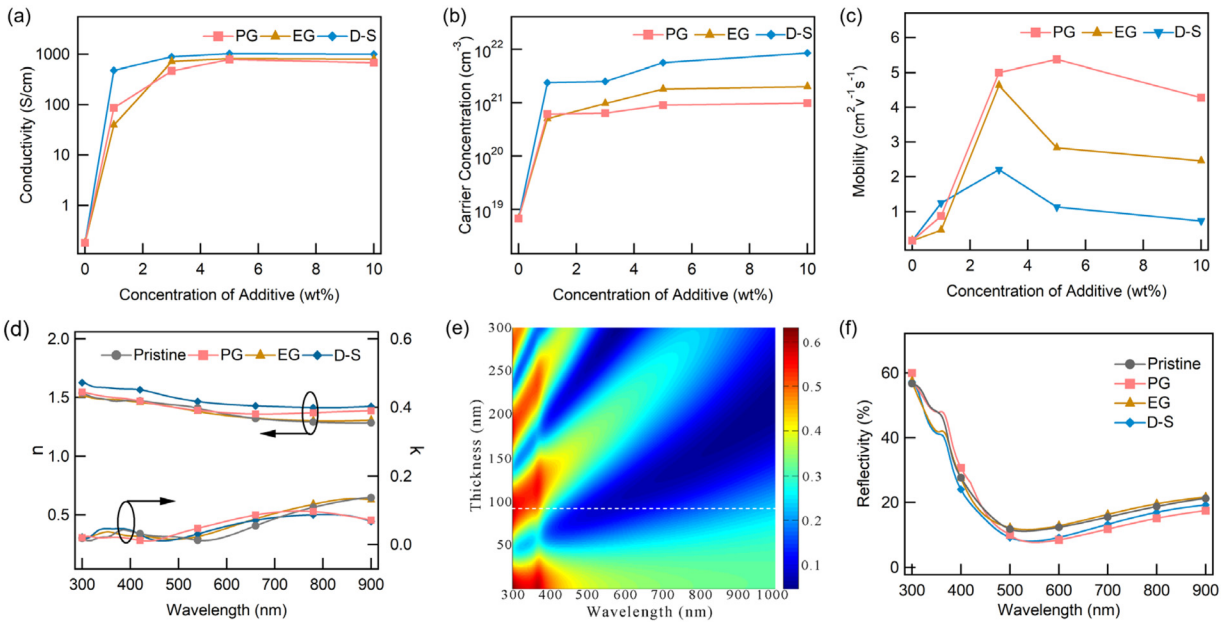

FIG. 3. (a)–(c) Electrical characteristics of PEDOT:PSS films as a function of different alcohol additive concentrations in precursor solution. (d) Optical constants of different alcohol-modified PEDOT:PSS films. (e) Simulated reflectance map of the semi-finished device with pristine PEDOT:PSS film. (f) Experimentally measured reflection spectra of different PEDOT:PSS films.

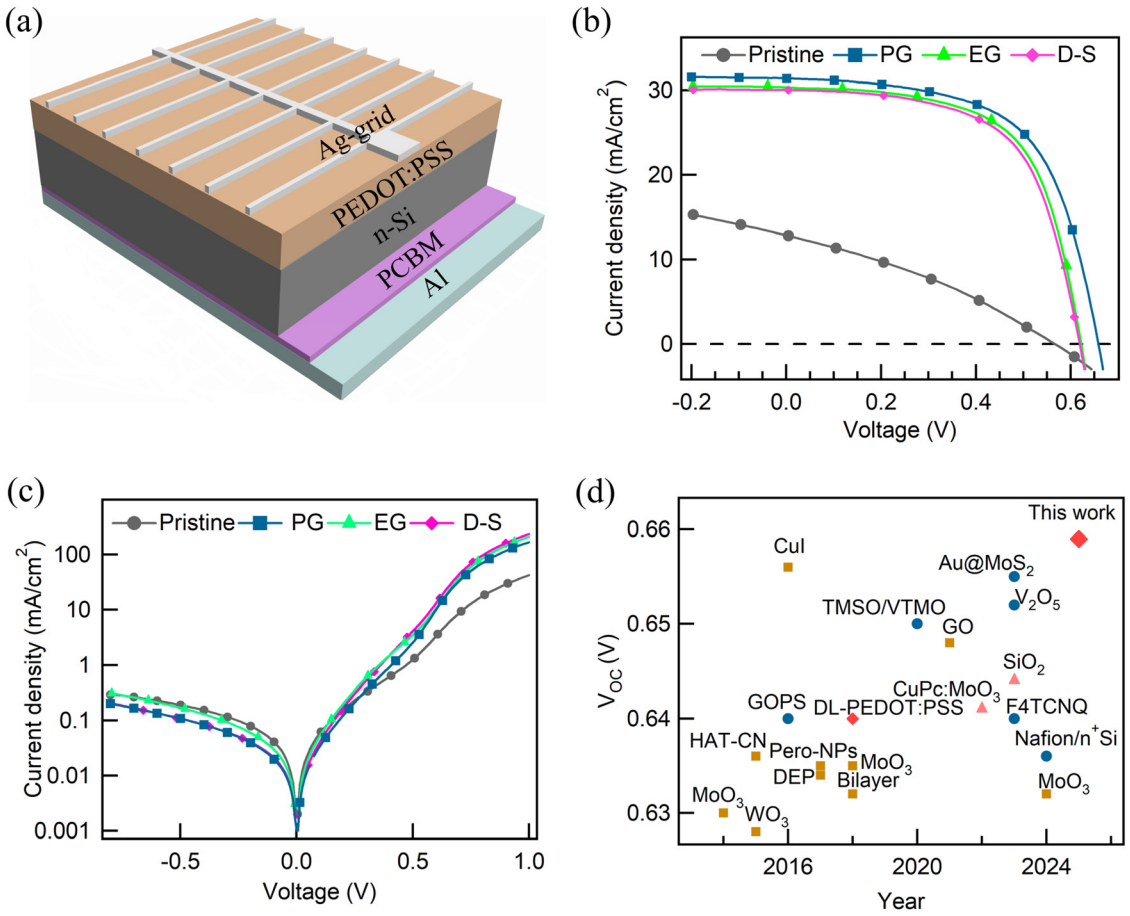

FIG. 4. (a) Schematic illustration of the PEDOT:PSS/Si HSCs structure. (b) The *J–V* characteristic curves of PEDOT:PSS/Si HSCs with different alcohol-modified PEDOT:PSS films. (c) The dark *J–V* characteristic curves of the PEDOT:PSS/Si HSCs. (d) The V_{OC} evolution of PEDOT:PSS/Si HSCs over the past 10 years.

indicating that the heterojunction possesses high quality and reduced leakage current. For comparison, Fig. 4(d) summarizes high V_{OC} values reported in the literature over the past decade for PEDOT:PSS/Si HSCs. This confirms the validity of the heterojunction theory and verifies that the band structure of the modified PEDOT:PSS films can serve to enhance the open-circuit voltage of the devices, thereby providing a feasible direction for improving device performance in future research.

The photovoltaic performance results can also be explained by the UPS data and capacitance–voltage (C–V) measurement results. Figure 5(a) shows the UPS spectra of PEDOT:PSS films modified with different alcohols, with molecular structures and compositions shown and discussed above in Fig. 1. The WF of PEDOT:PSS films was adjusted from 4.81 to 4.93 eV. The WF of PEDOT:PSS depends on both the bulk electrochemical potential of electrons within the film and the surface dipole, which is determined by PEDOT:PSS molecular structure and composition.[48,49] The variation in work function among different PEDOT:PSS samples can be ascribed to changes in the internal molecular structure of PEDOT and fluctuations in the PEDOT:PSS ratio. The V_{OC} is related to the magnitude of the built-in electric potential (V_{bi}).[4] C–V measurements were utilized to characterize the V_{bi} of the HSCs.[24,50,51] The plots of $1/C^2$-V are presented in Fig. S3. The HSCs with PG-modified PEDOT:PSS exhibit a high V_{bi} of 826 mV, which is 75 and 129 mV higher than those of the EG-modified and D-S-modified HSCs, respectively. The improved heterojunction parameters are consistent with the work function values measured by UPS measurements. Figure 5(b) presents the experimentally obtained energy level diagrams of PEDOT:PSS/n-Si contacts. As shown in Fig. 5(b), the PG-modified PEDOT:PSS films have the largest work function, which induces the greatest band bending magnitude and largest V_{OC} in the devices.

In conclusion, we have demonstrated that a simple doping method of PEDOT:PSS with alcohols of varying reducibility can precisely adjust the work function of PEDOT:PSS, which improves the quality of PEDOT:PSS/Si heterojunction. Characterization analysis and device performance reveal that high work function PEDOT:PSS induces a strong inversion layer on the Si surface and forms a high V_{bi} in PEDOT:PSS/Si HSCs. The performance of devices has significantly improved. The champion solar cell, based on PG-modified PEDOT:PSS, exhibits a record V_{OC} of 0.66 V. This thus offers a simple yet effective strategy to further enhance the V_{OC} of organic/silicon heterojunction devices.

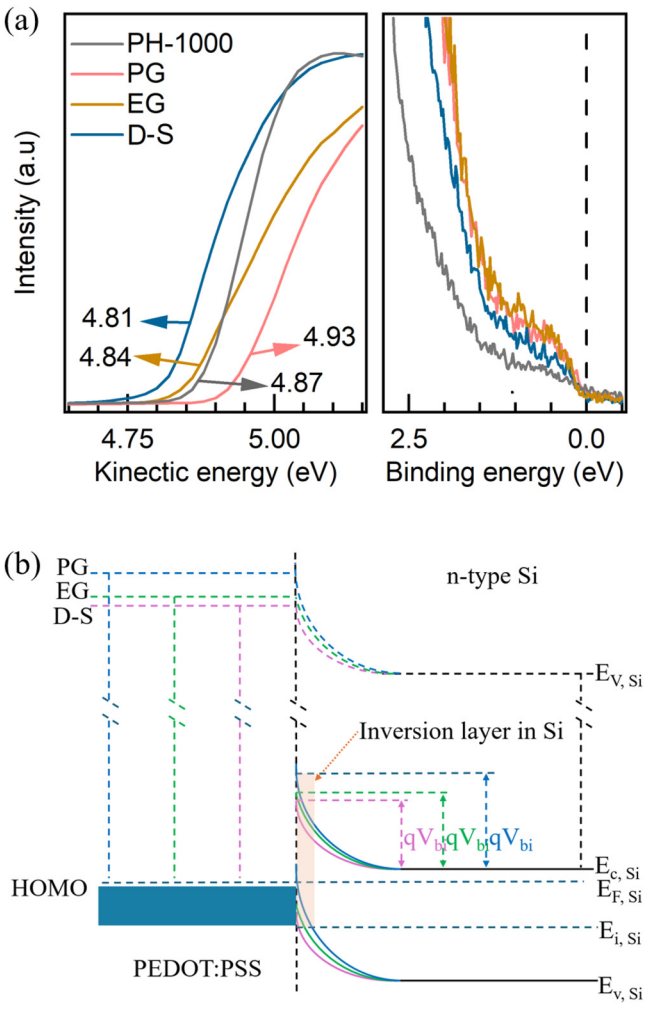

FIG. 5. (a) UPS spectra of alcohol-modified PEDOT:PSS films. (b) Energy band diagrams of PEDOT:PSS/Si heterojunctions derived from UPS spectra.

See the supplementary material for detailed methods of device fabrication, characterization, and measurement, along with supporting data. It includes experimental procedures, additional Raman and XPS spectra, reflection spectra as a function of film thickness, capacitance–voltage characteristics, and performance comparison tables. This material supports the findings presented in the manuscript.

This research was supported by the National Natural Science Foundation of China (12247166, 12474067, and 12074103) and the China Postdoctoral Science Foundation (2022M711070 and 2023M731019).

AUTHOR DECLARATIONS

Conflict of Interest

The authors have no conflicts to disclose.

Author Contributions

Leiming Yu: Conceptualization (equal); Data curation (equal); Formal analysis (equal); Funding acquisition (equal); Investigation (equal); Project administration (equal); Resources (equal); Supervision (equal); Writing – review & editing (equal). **Rui Yang:** Data curation (equal); Formal analysis (equal); Writing – original draft (equal). **Xiangdong Duan:** Data curation (equal); Formal analysis (equal). **Zhuo Wu:** Investigation (equal). **Suicai Zhang:** Project administration (equal); Resources (equal); Supervision (equal); Writing – review & editing (equal). **Xiaohui Song:** Conceptualization (equal); Methodology (equal); Project administration (equal). **Yurong Jiang:** Conceptualization (equal); Methodology (equal); Project administration (equal). **Congxin Xia:** Conceptualization (equal); Funding acquisition (equal); Project administration (equal); Resources (equal); Supervision (equal); Writing – review & editing (equal).

DATA AVAILABILITY

The data that support the finding of this study are available within the article and its supplementary material.

REFERENCES

[1]Y. Jiang, X. Dong, L. Sun, T. Liu, F. Qin, C. Xie, P. Jiang, L. Hu, X. Lu, X. Zhou, W. Meng, N. Li, C. J. Brabec, and Y. Zhou, Nat. Energy **7**(4), 352 (2022).
[2]J. Li, Y. Chen, Z. Fan, H. Liu, J. Liu, Z. Tan, S. Cao, K. Sun, Q. Liu, Z. Wang, L. Fang, and D. He, ACS Appl. Mater. Interfaces **17**(13), 19712 (2025).
[3]Z. B. Lu, J. H. Chen, Y. Y. Wu, H. Y. Wen, D. Chi, and S. H. Huang, Appl. Phys. Lett. **127**(9), 093901 (2025).
[4]R. B. Wang, Y. S. Wang, C. Wu, T. S. Zhai, J. C. Yang, B. Q. Sun, S. Duhm, and N. Koch, Adv. Funct. Mater. **30**(4), 1903440 (2020).
[5]H. Liu, Q. M. Liu, J. P. Liu, Y. G. Zhao, Y. J. Yu, Y. An, G. H. Wei, Y. Z. Li, Y. J. Fu, J. S. Li, and D. Y. He, Sol. Energy Mater. Sol. Cells **264**, 112624 (2024).
[6]Z. B. Lu, Y. Zhu, J. M. Chen, G. Z. Hou, H. C. Song, J. Xu, and K. J. Chen, Org. Electron. **108**, 106576 (2022).
[7]T. Gao, Q. Geng, Z. L. Gao, Y. F. Li, L. Chen, and M. C. Li, ACS Appl. Energy Mater. **4**(11), 12543 (2021).
[8]B. B. Chen, X. N. Zhang, Q. Gao, D. H. Yang, J. W. Chen, X. Chang, C. L. Zhang, Y. H. Bai, M. N. Cui, S. F. Wang, H. Li, B. S. Flavel, and J. H. Chen, Adv. Sci. **11**(12), 2306993 (2024).
[9]R. Li, X. Liu, and J. Chen, Exploration **3**(3), 20220027 (2023).
[10]Q. L. Jiang, J. B. Wu, C. Chen, Z. H. Su, Y. Z. Liu, L. Yang, B. C. He, X. Y. Gao, F. L. Gao, and L. F. Lu, Appl. Phys. Lett. **126**(10), 103902 (2025).
[11]Y. Q. Cui, J. Q. Wei, Y. C. Xiong, Q. Y. T. Shang, Q. Y. Liu, L. G. Huang, Y. Zhang, and W. Yu, J. Phys. Chem. C **128**(7), 2767 (2024).
[12]J. He, Y. M. Wan, P. Q. Gao, J. Tang, and J. C. Ye, Adv. Funct. Mater. **28**(34), 1802192 (2018).
[13]L.-M. Yu, T. Chen, N. Feng, R. Wang, T. Sun, Y. Zhou, H. Wang, Y. Yang, and Z.-H. Lu, Sol. RRL **4**(4), 1900513 (2020).
[14]Y. Sun, P. Gao, J. He, S. Zhou, Z. Ying, X. Yang, Y. Xiang, and J. Ye, Nanoscale Res. Lett. **11**(1), 310 (2016).
[15]R. Z. Shen, Z. H. Sun, Y. B. Shi, Y. R. Zhou, W. W. Guo, Y. Q. Zhou, H. Yan, and F. Z. Liu, ACS Nano **15**(4), 6296 (2021).
[16]W. B. Ji, T. Allen, X. B. Yang, G. S. Zeng, S. De Wolf, and A. Javey, ACS Energy Lett. **5**(3), 897 (2020).
[17]H. Lin, M. Yang, X. Ru, G. Wang, S. Yin, F. Peng, C. Hong, M. Qu, J. Lu, L. Fang, C. Han, P. Procel, O. Isabella, P. Gao, Z. Li, and X. Xu, Nat. Energy **8**(8), 789 (2023).
[18]Z. H. Sun, M. Liu, Y. R. Zhou, Q. Wang, Y. Yang, Y. Q. Zhou, and F. Z. Liu, Sol. Energy Mater. Sol. Cells **235**, 111453 (2022).
[19]B. K. Mondal, S. K. Mostaque, M. A. Rashid, A. Kuddus, H. Shirai, and J. Hossain, Superlattices Microstruct. **152**, 106853 (2021).
[20]B. Q. Liang, X. L. Chen, X. F. Wang, H. Z. Yuan, A. X. Sun, Z. Wang, L. Y. Hu, G. F. Hou, Y. Zhao, and X. D. Zhang, J. Mater. Chem. A **13**(4), 2441 (2025).
[21]Z. T. Luo, C. Yang, X. H. Chen, W. H. Ma, S. Y. Li, and K. X. Fu, J. Materiomics **9**(3), 438 (2023).
[22]Z. B. Lu, G. Z. Hou, J. M. Chen, J. Xu, and K. J. Chen, Sol. RRL **5**(8), 2100255 (2021).

[23]J. Y. Zhu, X. Yang, J. Sheng, P. Q. Gao, and J. C. Ye, ACS Appl. Energy Mater. **1**(6), 2874 (2018).
[24]Y. T. Mo, S. H. Xie, T. Y. Huang, R. B. Liao, J. H. Hu, F. S. Chen, W. T. Huang, J. F. Zhang, J. Chen, L. J. Sun, W. L. Wang, and G. Q. Li, Chem. Eng. J. **519**, 164889 (2025).
[25]Z. Sun, Y. He, B. L. Xiong, S. S. Chen, M. Li, Y. L. Zhou, Y. J. Zheng, K. Sun, and C. Yang, Angew. Chem., Int. Ed. **60**(10), 5036 (2021).
[26]Y. X. Cao, H. L. Liu, F. L. Gao, D. Y. Li, L. Xiang, J. W. Gao, P. Gao, Y. Zhang, and S. T. Li, Surf. Interfaces **37**, 102680 (2023).
[27]M. F. Abdelbar, M. El-Kemary, and N. Fukata, Nano Energy **77**, 105163 (2020).
[28]J. H. Chen, Z. B. Lu, X. T. Wang, Y. E. Luo, Y. Ma, G. Lou, D. Chi, and S. H. Huang, Nanomaterials **14**(20), 1630 (2024).
[29]J. He, P. Q. Gao, Z. H. Ling, L. Ding, Z. H. Yang, J. C. Ye, and Y. Cui, ACS Nano **10**(12), 11525 (2016).
[30]A. M. Ali, D. A. Said, M. Khayyat, M. Boustimi, and R. Seoudi, Results Phys. **16**, 102819 (2020).
[31]Y. T. Mo, C. Y. Guo, J. S. Guo, P. X. Liu, X. Wang, Y. F. Cai, J. Y. Chen, X. Deng, W. L. Wang, and G. Q. Li, J. Mater. Chem. A **12**(43), 29562 (2024).
[32]S. Mukherjee, A. Panigrahi, and A. Perumal, ACS Omega **10**(22), 23348 (2025).
[33]T. T. Yang, C. Xu, C. L. Liu, Y. Q. Ye, Z. W. Sun, B. Wang, and Z. Q. Luo, Chem. Eng. J. **429**, 132430 (2022).
[34]X. Fan, W. Nie, H. Tsai, N. Wang, H. Huang, Y. Cheng, R. Wen, L. Ma, F. Yan, and Y. Xia, Adv. Sci. **6**(19), 1900813 (2019).
[35]G. J. Zhang, H. Peng, Q. W. Wei, Z. Zhou, H. X. Wu, J. J. Luo, J. Wang, X. M. Wen, and Y. Yang, ACS Omega **9**(13), 15040 (2024).
[36]D. Won, J. Kim, J. Choi, H. Kim, S. Han, I. Ha, J. Bang, K. K. Kim, Y. Lee, T.-S. Kim, J.-H. Park, C. Y. Kim, and S. H. Ko, Sci. Adv. **8**(23), eabo3209 (2022).
[37]X. S. Rozhkova, A. K. Aimukhanov, B. R. Ilyassov, and A. K. Zeinidenov, Opt. Mater. **131**, 112708 (2022).
[38]M. Zeng, J. Ding, Y. Tian, Y. Zhang, X. Liu, Z. Chen, J. Sun, C. Wu, H. Yin, D. Wei, and H. Fan, Adv. Funct. Mater. **34**(52), 2411390 (2024).
[39]J. Wang, H. Yu, C. Hou, and J. Zhang, ACS Appl. Mater. Interfaces **12**(23), 26543 (2020).
[40]J. Hossain, Q. Liu, T. Miura, K. Kasahara, D. Harada, R. Ishikawa, K. Ueno, and H. Shirai, ACS Appl. Mater. Interfaces **8**(46), 31926 (2016).
[41]Y. Furukawa, J. Phys. Chem. **100**(39), 15644 (1996).
[42]I. Song, N. Y. Park, G. S. Jeong, J. H. Kang, J. H. Seo, and J. Y. Choi, Appl. Surf. Sci. **529**, 147176 (2020).
[43]B. Y. Ouyang, C. W. Chi, F. C. Chen, Q. F. Xi, and Y. Yang, Adv. Funct. Mater. **15**(2), 203 (2005).
[44]J. Ouyang, Q. Xu, C.-W. Chu, Y. Yang, G. Li, and J. Shinar, Polymer **45**(25), 8443 (2004).
[45]G. Zotti, S. Zecchin, G. Schiavon, F. Louwet, L. Groenendaal, X. Crispin, W. Osikowicz, W. Salaneck, and M. Fahlman, Macromolecules **36**(9), 3337 (2003).
[46]S.-M. Kim, C.-H. Kim, Y. Kim, N. Kim, W.-J. Lee, E.-H. Lee, D. Kim, S. Park, K. Lee, J. Rivnay, and M.-H. Yoon, Nat. Commun. **9**(1), 3858 (2018).
[47]Y. H. Kim, C. Sachse, M. L. Machala, C. May, L. Müller-Meskamp, and K. Leo, Adv. Funct. Mater. **21**(6), 1076 (2011).
[48]W. Shen, Y. He, Y. Chen, S. Chen, Z. Chen, C. Liu, H. Cui, S. Liu, L. Liu, G. Cheng, and S. Chen, Laser Photonics Rev. **19**(1), 2400707 (2025).
[49]Y.-J. Lin, F.-M. Yang, and C.-S. Lin, J. Appl. Phys. **102**(10), 103702 (2007).
[50]S. Kondratenko, V. Lysenko, Y. V. Gomeniuk, O. Kondratenko, Y. Kozyrev, O. Selyshchev, V. Dzhagan, and D. R. T. Zahn, ACS Appl. Energy Mater. **2**(8), 5983 (2019).
[51]J. Wang, W. J. Zhou, Q. W. Wei, G. S. Liu, X. B. Yuan, H. Pen, G. J. Zhang, R. F. Wang, C. Wang, and Y. Yang, Adv. Mater. Interfaces **10**(23), 2300187 (2023).

Supporting Information

Molecular Engineering of PEDOT:PSS for Enhancing Open-Circuit Voltage in Organic/Silicon Heterojunction Solar Cells

Leiming Yu, Rui Yang, Xiangdong Duan, Zhuo Wu, Suicai Zhang*, Xiaohui Song, Yurong Jiang, Congxin Xia*

School of Physics, Henan Key Laboratory of Advanced Semiconductor & Functional Device Integration, Henan Normal University, Xinxiang 453007, China

Author to whom correspondence should be addressed: zhangsuicai@htu.edu.cn, xiacongxin@htu.edu.cn

Experimental Section

Materials and Sample Preparation

PEDOT:PSS (Clevios PH-1000) aqueous solution was purchased from Heraeus, which has 1.2 wt% PEDOT:PSS solid in water, and the proportion of PEDOT and PSS is 1:2.5. EG, PG, and D-sorbitol alcohols and Triton X-100 surfactants were purchased from Sigma-Aldrich. Triton X-100 (0.2 wt%) was mixed into PEDOT:PSS (Clevios PH-1000) aqueous solution to improve its wettability. The mixed PEDOT:PSS solution was added with different mass ratios of alcohols (EG, PG, and D-s) to adjust the electrical properties and work function of PEDOT:PSS. Then, the doped PEDOT:PSS solution was ultrasonically shaken for 24 hours.

Device fabrication and characterization

Single-side polished, (100)-oriented, n-type single-crystal Si wafers with a thickness of 300 μm with a resistivity of 0.05–0.1 Ω·cm were used for photovoltaic devices fabrication and the sample for PEDOT:PSS film structure, morphology, and optical constant characterization. The Si substrates were cleaned by a standard RCA process. The Si substrates were dipped into 10 wt% HF aqueous solution for 1 min to remove the native oxide layer. For device fabrication, the doped PEDOT:PSS solution was spin-coated on the cleaned 1×1 cm^2 Si substrates and annealed at 130 °C for 15 min. The spin rate was slightly adjusted in the range of 2500–3000 rpm to minimize the reflection of the devices with various doping

PEDOT:PSS solutions. Subsequently, the Si substrates were transferred into the high vacuum evaporation system. The 200 nm Ag-grid front electrodes and 100 nm Al rear electrodes were deposited with a 0.1 nm/s deposition rate under 5.0×10^{-4} Pa vacuum conditions. The Ag-grid front electrode consists of one main grid and seven fine grids, whose coverage area is approximately 9% of the solar cells.

Characterization of the PEDOT:PSS Films

The structure and composition of different doped PEDOT:PSS films were characterized using Raman and XPS measurements. Raman spectra were acquired using a micro-Raman system (Renishaw, India) with an Nd:YAG laser source (λ = 514.5 nm), an integration time of 60 s, and a power of 20 mW at the film surface. XPS measurements were performed using a monochromatic Al Kα source (1486.6 eV) and a hemispherical analyzer in a high-vacuum chamber with a base pressure of 2×10^{-7} mbar. The morphology of the PEDOT:PSS films was analyzed using field-emission scanning electron microscopy (FESEM, Nova Nano SEM 450) and atomic force microscopy (AFM, SPA-400). The current density-voltage (J-V) characteristics of the PEDOT:PSS/Si HSCs were measured with a Keithley 2400 source meter under simulated AM1.5 G illumination (100 mW/cm²), calibrated with a standard monocrystalline silicon reference cell (PV Measurements). The capacitance versus voltage (C-V) curves were measured at a frequency of 100 kHz using a Keithley B1500

semiconductor parameter analyzer, with the bias voltage sweep from -1 V to 1 V. A copper metal light-passing window (9×9 mm^2) was used to define the active area. Optical simulations of the devices were performed in MATLAB based on the transfer-matrix theory. The initial data for the simulation included the layer thicknesses and optical constants, the latter of which were measured by spectroscopic ellipsometry. A multilayer stack model of Air/PEDOT:PSS/Si (300 μm)/PCBM (30 nm)/Al (100 nm)/Air was established. The device's reflection spectrum was simulated using a transfer-matrix method (TMM) program written in MATLAB, which incorporated the measured optical constants and thicknesses of all layers.

Table S1: Electrical output characteristics of devices for representative high V_{OC} PEDOT:PSS/Si hybrid heterojunction solar cells.

Device structure	Modification	Si Structure	V_{OC} (mV)	J_{SC} (mA/cm^2)	FF (%)	PCE (%)	Year	Ref.
TiO_2/Ag-grid/PEDOT:PSS/ n-Si/ InGa	EG/Zonyl fluorosurfactant/ DMSO/PTSA	Plane	620	34.3	73	15.5	2015	1
Ag-grid/PEDOT:PSS/n-Si/Al	DMSO/Triton X-100/GOPS	SiNWs	640	30.2	72.8	14.1	2016	2
Ag-grid/HC-PEDOT:PSS/HA-PEDOT:PSS/n-Si/CPTA/Al	DMSO/Triton X-100/GOPS/EMIM-TCM	Pyramid	632	34.7	76.3	16.7	2018	3
Ag-grid/PEDOT:PSS/n-Si/ Ti-Ag	DMSO/isopropanol /Mn-$CsPbCl_3$	Nanotips	560	37.79	63	13.48	2020	4
Ag-grid/PEDOT:PSS/n-Si/P(VDF-TrFE)/Al	EG/Triton X-100	Nanocone	645	37.72	75.5	18.37	2020	5
Ag-grid/AgNWs/PEDOT:PSS/n-Si/PCBM/Mg/Al	DMSO/Triton X-100/TMOS/VTMO	SiNWs	650	34.8	80.1	18.12	2021	6
Ag-grid/PEDOT:PSS/TS-CuPc:MoO_3/n-Si/TiN/Al	DMSO/Triton X-100	SiNWs	641	34.10	73.54	16.09	2022	7
Ag-grid/PEDOT:PSS/SiO_2/n-Si/P(VDF-TrFE)/Al	EG/Triton X-100	Plane	644	17.23	73.7	8.18	2023	8
Ag-grid/PEDOT:PSS/PEDOT:PSS-Nafion /n-Si/InGa	EG/Triton X-100/Nafion/DBSA-Methanol	Plane	600	29.07	70.67	12.33	2023	9
Ag-grid/PEDOT:PSS-Nafion/n-Si/ SiO_2/n^+-poly-Si/Al	DMSO/Triton X-100/Nafion	Plane	636	31.1	69.1	13.7	2024	10
Ag-grid/PEDOT:PSS/n-Si/PCBM/Al	PG/Triton X-100	Plane	660	32.36	59.97	12.80	This work	

Table S2: Electrical output characteristics of PEDOT:PSS/Si hybrid heterojunction solar cells with different doping modification.

Type	V_{OC} (V)	J_{SC} (mA/cm²)	FF (%)	PCE (%)	R_S (Ω/cm²)
Pristine	**0.558**	**12.05**	**28.28**	**1.90**	**29.24**
	(0.473±0.095)	(10.87±1.18)	(37.35±8.5)	(1.86±0.21)	(28.73±5.32)
Propylene glycol	**0.660**	**32.36**	**59.97**	**12.80**	**8.67**
	(0.651±0.013)	(31.41±0.78)	(61.02±3.44)	(12.49±0.3)	(5.30±3.94)
Ethylene glycol	**0.621**	**30.31**	**62.18**	**11.71**	**1.88**
	(0.617±0.005)	(28.99±3.58)	(60.08±2.10)	(10.75±0.27)	(1.51±1.87)
D-Sorbitol	**0.618**	**30.01**	**61.12**	**11.35**	**2.63**
	(0.614±0.004)	(28.73±1.28)	(60.55±2.54)	(10.70±0.65)	(4.63±2.04)

Note: Data and statistics were obtained from 10 devices under each condition. The numbers in bold are the champion values.

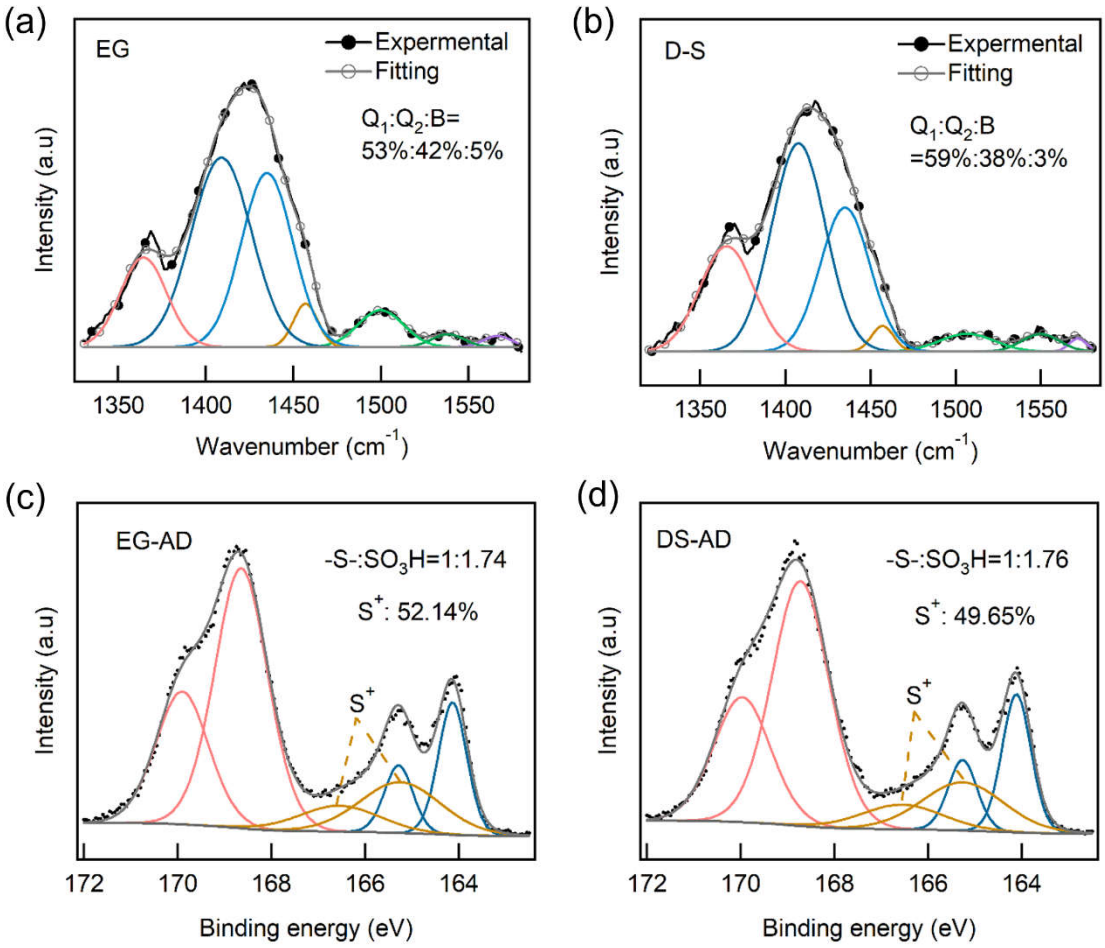

Fig. S1. (a, b) Peak-fitting analysis of the Raman spectra and (c, d) XPS spectra of the S 2p core-level region for the modified PEDOT:PSS films: (a, c) EG-modified; (b, d) D-S-modified.

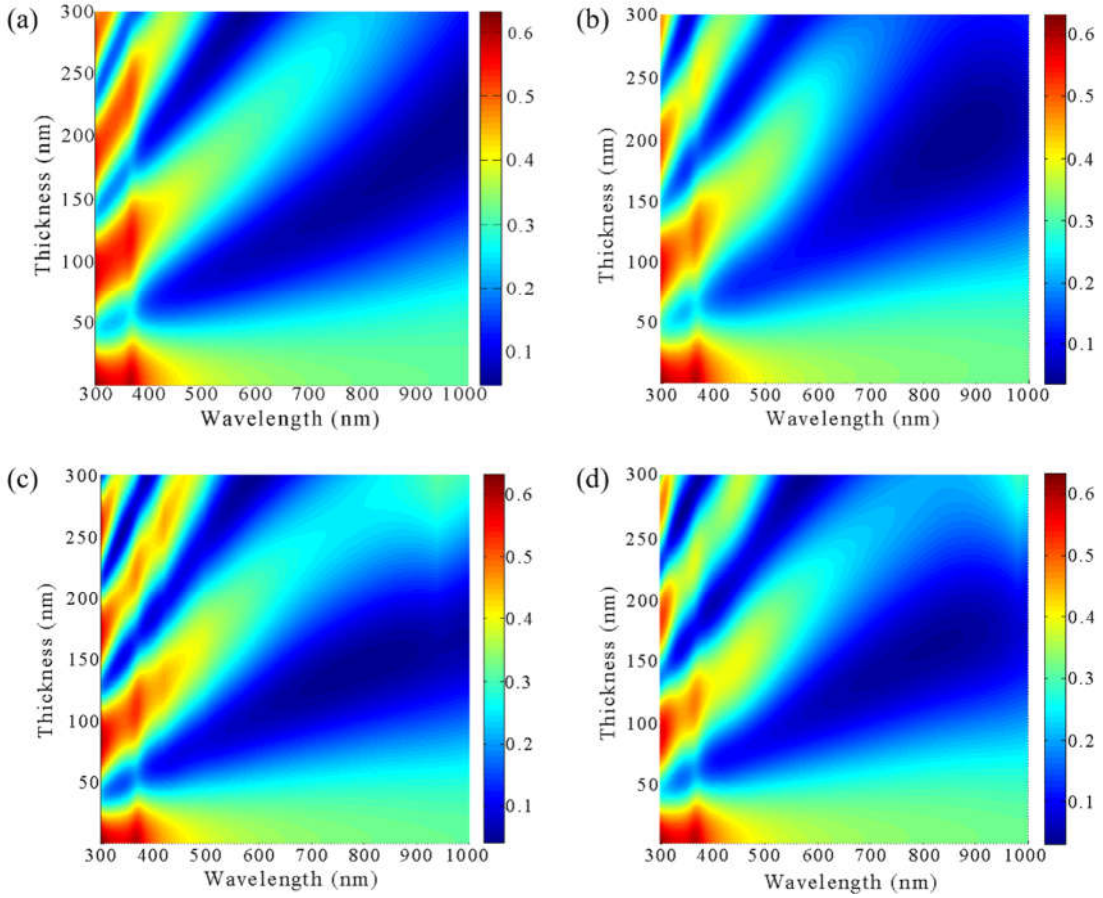

Fig. S2. Reflection spectra of alcohol-modified PEDOT:PSS films as a function of thickness: (a) PH-1000, (b) Ethylene glycol, (c) Propylene glycol, (d) D-Sorbitol

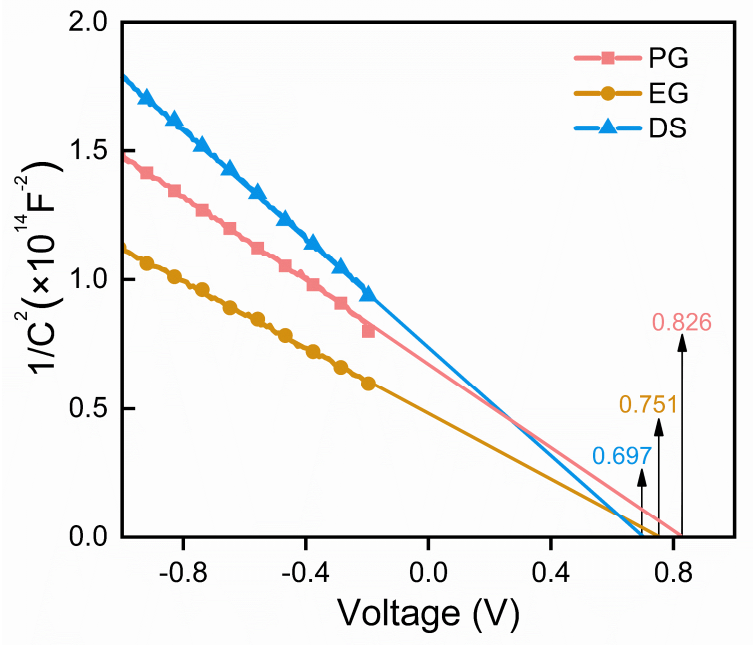

Fig. S3. Capacitance–voltage curves of PEDOT:PSS/n-Si heterojunctions with different alcohol-modified PEDOT:PSS films.

References

[1] Q. M. Liu, R. Ishikawa, S. Funada, T. Ohki, K. Ueno, and H. Shirai, Adv. Energy Mater. **5** (17), 1500744 (2015).

[2] S. Wu, W. Cui, N. Aghdassi, T. Song, S. Duhm, S. T. Lee, and B. Q. Sun, Adv. Funct. Mater. **26** (28), 5035 (2016).

[3] J. He, Y. M. Wan, P. Q. Gao, J. Tang, and J. C. Ye, Adv. Funct. Mater. **28** (34), 1802192 (2018).

[4] M. F. Abdelbar, M. El-Kemary, and N. Fukata, Nano Energy. **77**, 105163 (2020).

[5] S. B. Kang, W. J. Park, M. H. Jeong, S. H. Kang, C. Yang, and K. J. Choi, Adv. Funct. Mater. **30** (50), 2004943 (2020).

[6] R. Z. Shen, Z. H. Sun, Y. B. Shi, Y. R. Zhou, W. W. Guo, Y. Q. Zhou, H. Yan, and F. Z. Liu, ACS Nano. **15** (4), 6296 (2021).

[7] Z. B. Lu, Y. Zhu, J. M. Chen, G. Z. Hou, H. C. Song, J. Xu, and K. J. Chen, Org. Electron. **108**, 106576 (2022).

[8] Y. Yang, D. Su, N. X. Jin, F. H. Liu, X. Y. Zhang, P. Xia, Y. J. Song, H. L. Zhou, W. P. Wu, and T. Zhang, Sol. RRL. **7** (24), 2300627 (2023).

[9] Y. Wang, W. Z. Jiang, Y. G. Zhao, M. Z. Lv, Y. An, Y. Wang, Q. Zhang, H. Liu, C. X. Liu, Z. N. Fan, Q. M. Liu, and D. Y. He, PHYS STATUS SOLIDI-R. **17** (10), 2300086 (2023).

[10] Y. Cui, J. Wei, Y. Xiong, Q.-Y. T. Shang, Q. Liu, L. Huang, Y. Zhang, and W. Yu, J. Phys. Chem. C. **128** (7), 2767 (2024).